Nanotechnology

PAPER • OPEN ACCESS

Carbon nanotubes assembled on porous TiO_2 matrix doped with Co_3O_4 as sulfur host for lithium–sulfur batteries

To cite this article: Weilong Qiu *et al* 2021 *Nanotechnology* **32** 075403

OPEN ACCESS
IOP Publishing
Nanotechnology

Nanotechnology **32** (2021) 075403 (8pp)
https://doi.org/10.1088/1361-6528/abc451

Carbon nanotubes assembled on porous TiO_2 matrix doped with Co_3O_4 as sulfur host for lithium–sulfur batteries

Weilong Qiu[1], Jing Li[1], Yongguang Zhang[1,*], Gulnur Kalimuldina[2] and Zhumabay Bakenov[3,*]

[1] School of Materials Science and Engineering, Hebei University of Technology, Tianjin 300130, People's Republic of China
[2] Department of Mechanical and Aerospace Engineering, Nazarbayev University, Nur-Sultan, 010000, Kazakhstan
[3] Department of Chemical and Materials Engineering, National Laboratory Astana, Nazarbayev University, Institute of Batteries LLP, Nur-Sultan, 010000, Kazakhstan

E-mail: yongguangzhang@hebut.edu.cn and zbakenov@nu.edu.kz

Received 2 September 2020, revised 3 October 2020
Accepted for publication 23 October 2020
Published 24 November 2020

Abstract

Advanced design and fabrication of high performance sulfur cathodes with improved conductivity and chemical adsorption towards lithium polysulfides (LiPS) are crucial for further development of Li–S batteries. Hence, we designed a TiO_2/Co_3O_4-CNTs composite derived from Ti-MOF (MIL-125) as the host matrix for sulfur cathode. The polar nature of metal oxides (TiO_2, Co_3O_4) creates the adsorptive sites in the composite and leads to an efficient chemical capture of LiPS. The CNTs ensure the contact between S/Li_2S and the host material with high conductivity, enhanced charge transfer and fast electrochemical kinetics. At the same time, the CNTs strengthen the stability of the electrode material. Consequently, the as-prepared TiO_2/Co_3O_4-CNTs composite showed excellent electrochemical performance. The cell with S–TiO_2/Co_3O_4-CNTs delivers an initial specific capacity of 1270 mAh g^{-1} at 0.2 C and high rate performance with a capacity of 603 mAh g^{-1} at 3 C.

Supplementary material for this article is available online

Keywords: porous carbon matrix, lithium–sulfur battery, polysulfides shuttle effect, low-cost and facile synthesis, titanium metal-organic framework

1. Introduction

Lithium-ion batteries (LIBs) have claimed the seat of a leader in the energy storage system technologies today. However, since conventional LIBs have almost reached their performance limits, the emerging alternative rechargeable battery types as lithium–sulfur battery (Li–S), Li-air and some other are attracting an extraordinarily high interest of researchers [1, 2]. Among these batteries, the Li–S system is being especially intensively studied to enclose its needed commercialization. Sulfur has the electrochemical capability of multi-electron reduction reaction and low molecular weight of 32 g mol^{-1}. These properties provide Li–S batteries with high theoretical capacity (1600 mAh g^{-1}) and energy density (2500 Wh kg^{-1}) [3, 4]. That makes Li–S batteries fivefold more powerful than the conventional LIBs. Despite outstanding theoretical electrochemical properties, Li–S batteries still have problems impeding their practical application. First of all, the conductivity of elemental sulfur is low at room temperature ($\Omega = 5 \times 10^{-30}$ S cm^{-1} at 25 °C), which makes difficult the activation process of the sulfur-based cathode

* Authors to whom any correspondence should be addressed.

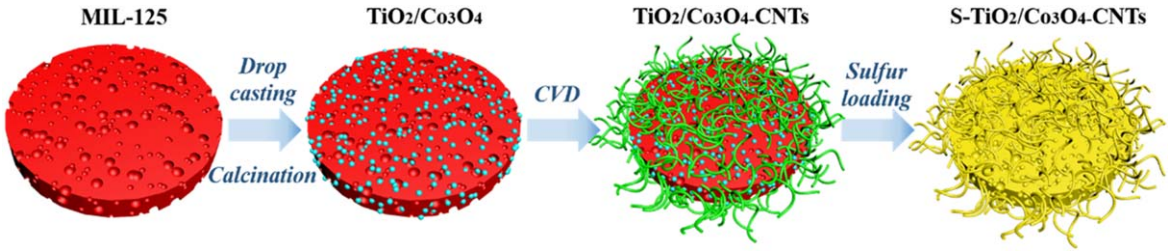

Figure 1. Schematics of S–TiO_2/Co_3O_4-CNTs composite preparation.

material [5, 6]. Secondly, during charge/discharge processes, the generated polysulfide (PS) is easily dissolved in the electrolyte and migrates to the lithium anode. It reacts with lithium forming lithium polysulfide LiPS, which produces a 'shuttle effect' leading to an irreversible loss of active material [7–9]. The effective strategies are urgently needed to solve these issues.

In the last two decades, many research groups have proposed various methods to mitigate the issues of the Li–S batteries mentioned above. Among them, the incorporation of highly conductive carbon as a sulfur host material is considered one of the most effective. Such hosts could enhance the conductivity of sulfur composite and reduce the LiPS shuttle. Therefore, various carbon materials like graphene [10], porous carbon [11], and carbon nanotubes [12, 13] were intensively studied for application in Li–S batteries. However, yet the issues come with the nonpolar nature of carbon, which leads to its weak interaction with polar LiPS. As a result, the poor interaction between carbon and LiPS reduces the effectiveness of capturing soluble LiPS and reducing their shuttle. In addition, the high cost of the carbon materials used and the complexity of their synthesis limits the possibilities of their practical application in the energy storage system [14, 15].

On the other hand, the metal oxides (TiO_2 [16, 17], MnO_2 [18, 19], and Co_3O_4 [20, 21]) with polar surfaces were reported to form strong chemical bonds with the LiPS. Due to this capability, the metal oxide structures was proved to be an effective means to reduce the LiPS dissolution. However, the low specific surface area and poor conductivity of the metal oxides make it challenging to increase the sulfur mass loading.

The porous materials as hosts/carriers for active components have been extensively studied for various applications requiring the system activity enhancement due to the abundance of active sites [22–24]. For example, Hussain *et al* synthesized a novel Ni_9S_8/C electrocatalyst for methanol oxidation reaction (MOR) [22]. It was proved that Ni_9S_8 embedded in porous carbon carrier exhibits enhanced performance due to the availability of effective active sites for MOR. Lu *et al* synthesized a composite consisting of cobalt and graphitic porous carbon Co@GC-PC from bimetallic metal–organic frameworks as a new sulfur body for high-performance Li–S batteries [23]. A highly reversible capacity of 790 mAh g^{-1} at 0.2 C after 220 cycles was achieved for the Li–S batteries when the Co@GC-PC was used as the sulfur host. Similarly, Wang *et al* prepared porous carbon nanotubes as the host of the sulfur cathode by doping with nitrogen and integrating a highly dispersed cobalt catalyst [24]. The host structure derived from MOF enabled a high performance Li–S battery with a long cycle life (86% of the capacity retention within 500 cycles) and high rate performance (600 mAh g^{-1} at a high current density of 7.5 A g^{-1}).

In this work, we designed a TiO_2/Co_3O_4-carbon nanotubes (CNTs) composite derived from titanium metal-organic framework (Ti-MOF, MIL-125) as the substrate for sulfur hosting. The fabricated porous TiO_2 matrix provides sufficient pore volume to store sulfur and buffer its volume expansion during the charge/discharge process. In addition, Co_3O_4 nanoparticles with strong polarity activate enhanced interactions with PSs and have a variety of adsorption and electrocatalytic sites, which can promote the conversion reaction of intermediate LiPS. Furthermore, the CNTs improve contact between S/Li_2S and host material and strengthen the structural integrity and stability of the composite cathode.

2. Experimental section

2.1. Preparation of S–TiO_2/Co_3O_4 and S–TiO_2/Co_3O_4-CNTs electrodes

Initially, 1 mmol titanium isopropoxide $Ti(OiPr)_4$ and 1.5 mmol terephthalic acid were dissolved in a 5 ml mixture of methanol and dimethylformamide (DMF) with a volume ratio of 1:9. After stirring for 5 min, the mixed solution was transferred and kept in the autoclave reactor for 15 h at 150 °C. After a consequent cooling of the reactor to room temperature, the precipitated powder was collected and washed twice with acetone. Finally, the MIL-125 was obtained after annealing the powder at 200 °C for 12 h.

As shown in figure 1, the TiO_2 was prepared by heated MIL-125 at 500 °C for 2 h. After that, the TiO_2 was immersed in a $Co(CH_3COO)_2$ solution (0.2 M) for 30 min, and the obtained product was annealed at 500 °C for 50 min to synthesize TiO_2/Co_3O_4.

TiO_2/Co_3O_4-CNTs was prepared by a typical chemical vapor deposition (CVD) method [25]. The TiO_2/Co_3O_4 was heated in a tubular furnace to 600 °C (5 °C min^{-1}) in a mixture of H_2 and Ar gasses with a gas flow of 10 and 80 ml min^{-1}, respectively, and *in situ* reduced at this temperature for 30 min. Afterwards, at the same H_2/Ar flow ratio maintained, 10 ml min^{-1} acetylene (C_2H_2) was fed as a carbon

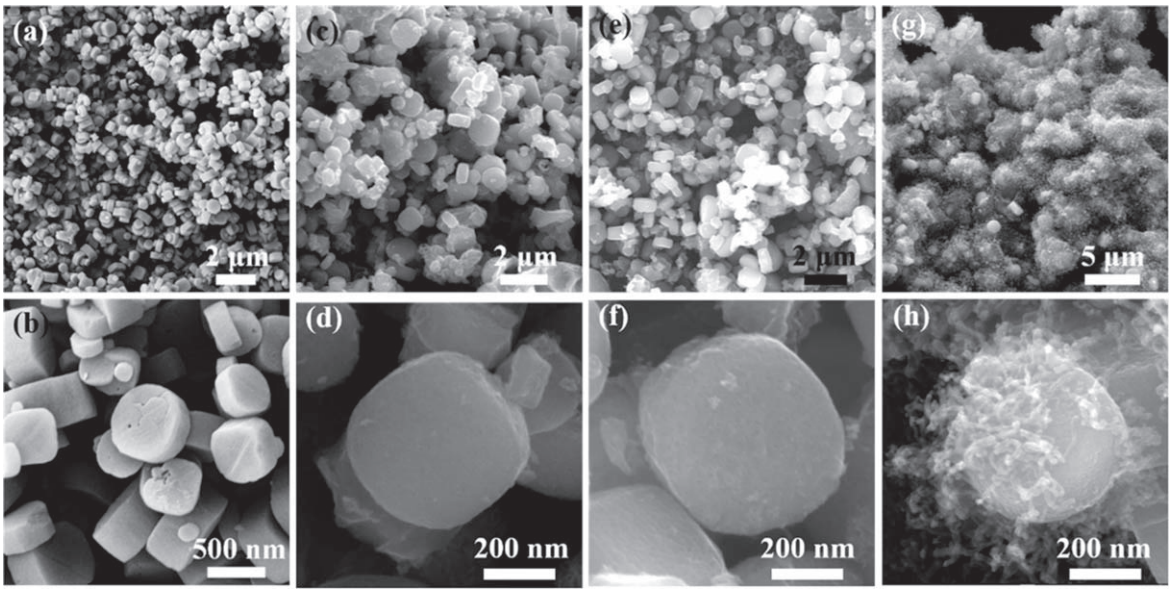

Figure 2. SEM images of (a), (b) MIL-125, (c), (d) TiO_2, (e), (f) TiO_2/Co_3O_4 and (g), (h) TiO_2/Co_3O_4-CNTs.

source for 20 min to grow carbon nanotubes on TiO_2/Co_3O_4. The TiO_2/Co_3O_4-CNTs was obtained after cooling the product to room temperature in Ar gas. Finally, TiO_2/Co_3O_4-CNTs and S powder were mixed (w/w = 1:3) and heat treated at 155 °C for 12 h to obtain the S–TiO_2/Co_3O_4-CNTs composite. In parallel experiments, the S–TiO_2/Co_3O_4 composite was obtained via a similar procedure but without the CVD process.

2.2. Material characterization

The morphology and structure of samples were investigated by field emission scanning electron microscopy (FE-SEM, SIGME 500) coupled with energy dispersive spectroscopy (EDS), and high-resolution transmission electron microscopy (HR-TEM, JEM-2100F, JEOL). X-ray diffraction (XRD) patterns were obtained by Bruker D8 diffractometer equipped with Cu-Ka radiation source. The N_2 adsorption/desorption tests were carried out to measure the porosity and specific surface area at 77 K by a V-Sorb 2800P surface area and pore distribution Brunauer–Emmett–Teller (BET) analyzer instrument. X-ray photoelectron spectroscopy (XPS, Thermo Fisher Scientific, ESCALAB 250Xi, USA) was used to analyze the elements and valence states of the samples.

2.3. Electrochemical evaluation

Electrochemical properties of the samples were studied using a 2032 coin-type cell, where a piece of Li foil with a thickness of 1.0 mm was used as both a reference and anode. The separator was the Celgard 2300, and the electrolyte was composed of 1.0 mol l^{-1} of LiTFSI in a mixed solvent of 1,3-dioxolane (DOL) and dimethyl ether (DME) (v/v = 1:1) with 1 wt% lithium nitrate ($LiNO_3$). The amount of electrolyte used in the cell was precisely controlled at an electrolyte/sulfur ratio of 15 μl (electrolyte)/mg (S). The cells were galvanostatically cycled within the cut-off potential range of 1.7–2.8 V versus Li/Li^+ on a Land battery tester under different current rates (1 C = 1675 mA g^{-1}). Cyclic voltammetry (CV) curves were recorded on a Versa STAT4 electrochemical workstation (Princeton Applied Research) at a scanning rate of 0.1 mV s^{-1}.

3. Results and discussion

The SEM images demonstrating the morphology of the samples are shown in figure 2. It can be observed that the synthesized MIL-125 has a well-defined disc-like structure with an average diameter of the disks about 500 nm (figures 2(a) and (b)). Figures 2(c) and (d) demonstrate the TiO_2 particles after heat treatment at 500 °C for 2 h in air. It can clearly be seen that TiO_2 maintains its morphology with a visible slight roughening of the surface. It can be seen from figures 2(e) and (f) that the morphology of the further prepared TiO_2/Co_3O_4 was similar to TiO_2, without the appearance of distinct and large particles of Co_3O_4. Such results suggest that Co_3O_4 was uniformly deposited within the porous structure of TiO_2 obtained from MIL-125. The following CVD process resulted in the vertical growth of CNT tentacles which can be seen on the surface of TiO_2/Co_3O_4 (figures 2(g) and (h)). The final TiO_2/Co_3O_4-CNTs particles have larger void spaces than MIL-125 due to the presence of CNTs, which is favorable and suitable to act as a conductive area for sulfur loading. Moreover, such structure with the conductive CNTs can further promote fast electron transfer and efficaciously alleviate the electrode volume expansion during charge/discharge processes.

The structure of the obtained TiO_2/Co_3O_4-CNTs was analyzed by TEM. As shown in figure 3(a), we could confirm the vertical growth of CNTs on the surface of TiO_2/Co_3O_4. The EDS mapping of TiO_2/Co_3O_4-CNTs showed that Co, O, Ti and C were uniformly distributed in the sample

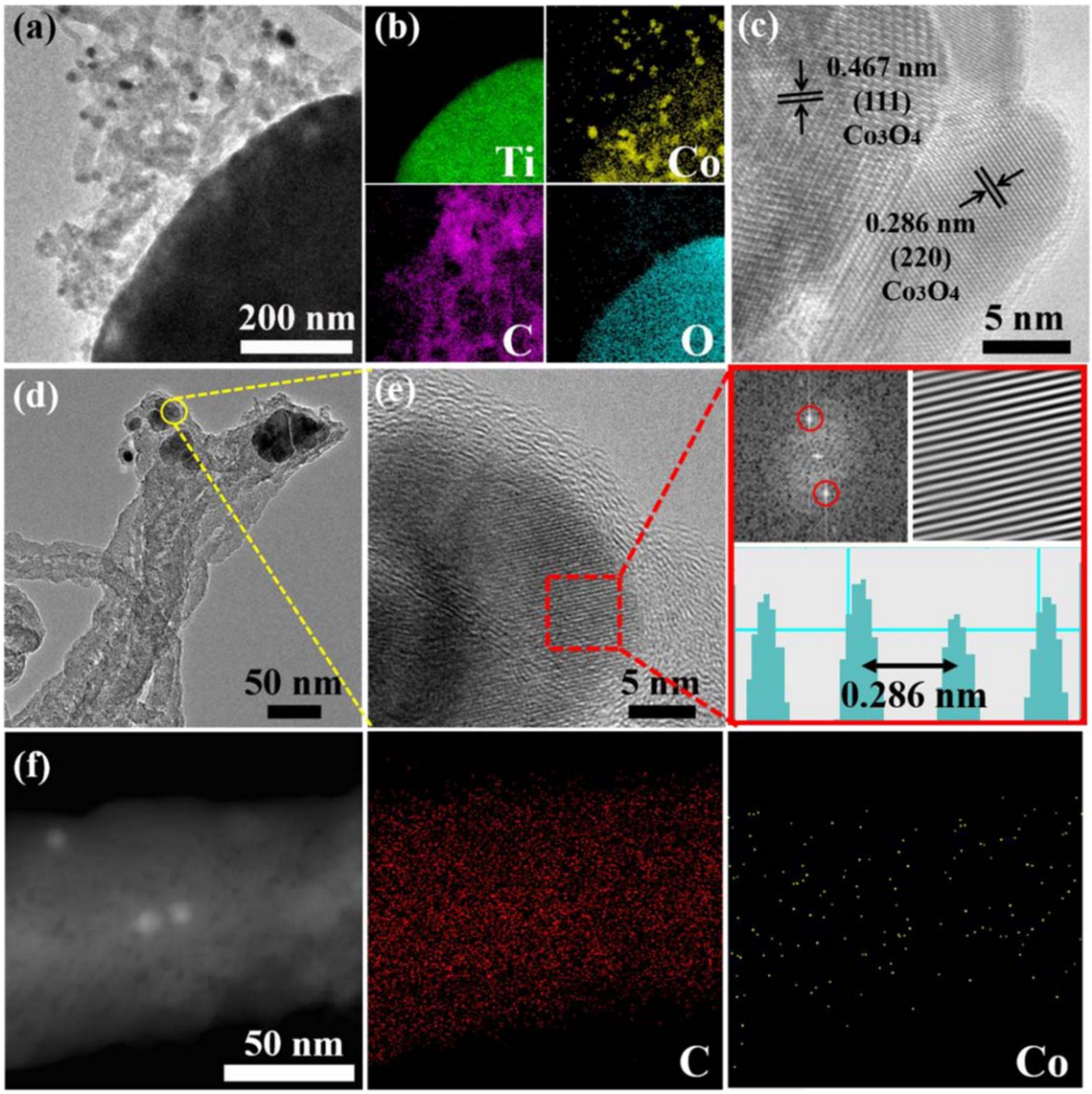

Figure 3. TEM image of (a) TiO_2/Co_3O_4-CNTs; (b) EDS mapping of TiO_2/Co_3O_4-CNTs; (c), (d) HRTEM images of TiO_2/Co_3O_4-CNTs; (e) FFT pattern, inverse FFT image and the lattice spacing profiles of TiO_2/Co_3O_4-CNTs; (f) EDS mapping of single CNT.

(figure 3(b)). These results demonstrate that some amount of Co_3O_4 is also distributed on the CNTs' side. The HRTEM results also demonstrate the presence of crystalline particles on the CNTs' side (figures 3(c) and (d)). The lattice fringes with mirror spacings of 0.467 and 0.286 nm in the HRTEM image (figure 3(d)) of a nanoparticle on CNT can be corresponded to the (111) and (220) crystal plane of Co_3O_4, respectively. On the other hand, further analysis of the CNTs by FFT and inverse FFT (figure 3(e)) showed that the Co_3O_4 particles were embedded on the top of the CNTs. Figure 3(f) presents the EDS elemental mapping of a single CNT for C and Co. These results confirm that superfine particles of Co_3O_4 exist on CNTs as well.

As shown in figure 4(a), the peaks of rutile TiO_2 and anatase TiO_2 were obviously observable in both TiO_2/Co_3O_4 and TiO_2/Co_3O_4-CNTs composites. After the addition of sulfur, the most exhibited sharp diffraction peaks in the XRD patterns of the S–TiO_2/Co_3O_4-CNT composite correspond to the characteristic peaks of S_8. On the contrary, the diffraction peaks of TiO_2 have less intensity in this case. The comparative studies of the porous textures of the TiO_2 and TiO_2/Co_3O_4 samples were conducted by the N_2 adsorption–desorption method. As shown in figure S1 is available online at stacks.iop.org/NANO/32/075403/mmedia, both TiO_2 and TiO_2/Co_3O_4 exhibit a typical type-IV isotherm curve with a BET surface area of 29.2 $m^2 g^{-1}$ and 36.6 $m^2 g^{-1}$, respectively. Furthermore, the N_2 adsorption/desorption curves and pore-size distribution of the TiO_2/Co_3O_4-CNTs and S–TiO_2/Co_3O_4-CNTs samples by BET analysis are shown in figures 4(b) and (c). The measurements showed that TiO_2/Co_3O_4-CNTs has a BET surface area of 110.8 $m^2 g^{-1}$ and a pore volume of 0.16 $cm^3 g^{-1}$. Due to the introduction of CNTs, the BET surface area of TiO_2/Co_3O_4-CNTs was significantly increased, which is favorable for providing

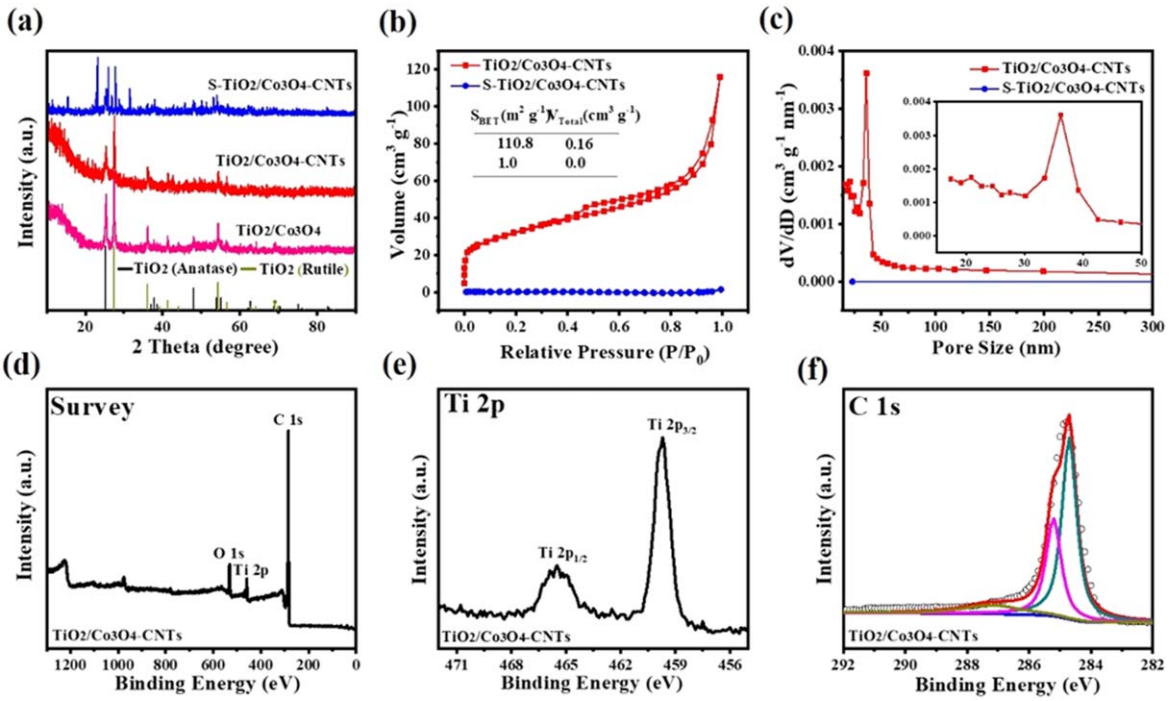

Figure 4. (a) XRD patterns of TiO_2/Co_3O_4, TiO_2/Co_3O_4-CNTs and S–TiO_2/Co_3O_4-CNTs; (b), (c) N_2 adsorption/desorption isotherms and pore size distribution of TiO_2/Co_3O_4-CNTs and S–TiO_2/Co_3O_4-CNTs; (d) XPS full spectrum, and high-resolution XPS spectra of (e) Ti 2p and (f) C 1s for TiO_2/Co_3O_4-CNTs.

sufficient sites for the adsorption of LiPS. These values were significantly reduced after loading sulfur, suggesting that sulfur was successfully embedded within the mesopores of TiO_2/Co_3O_4-CNTs. It can be concluded from figure 4(c) that largely mesoporous TiO_2/Co_3O_4-CNTs can be effective not only for constraining the shuttle of LiPS but could also facilitate enhanced transport and diffusion of ions.

To further probe the bonding characteristics and surface chemical composition of TiO_2/Co_3O_4-CNTs the XPS analysis was performed (figures 4(d)–(f)). The XPS survey in figure 4(d) confirms the elemental composition showing sharp characteristic peaks of Ti, O, C. Notably, two peaks at 465.5 eV and 459.4 eV were observed in the spectra of Ti 2p, which corresponds to the Ti $2p_{1/2}$ and Ti $2p_{3/2}$, respectively (figure 4(e)) [26, 27]. In the C 1s spectrum (figure 4(f)), the peaks at 284.8 eV, 285.6 eV and 287.4 eV were consistent with the C–C, C=O and C–O bonds, respectively [28, 29].

To verify the strong surface affinity of TiO_2/Co_3O_4-CNTs toward LiPS adsorption, and to compare the adsorption behavior of CNTs, TiO_2/Co_3O_4 and TiO_2/Co_3O_4-CNTs the facile visual adsorption tests were conducted (figure S2). The same weight sample of each of the powders was soaked in a Li_2S_6 solution. The inset shows that initially light brown solution became colorless after mixing with TiO_2/Co_3O_4-CNTs for 24 h, indicating that the TiO_2/Co_3O_4-CNTs composite completely adsorbed the Li_2S_6 from the solution. On the other hand, the solution with immersed TiO_2/Co_3O_4 and CNTs samples just turned its color to a faint yellow. The UV–vis adsorption spectra of the test solutions also indicated that TiO_2/Co_3O_4-CNTs shows an obvious reduction of absorbance, proving the excellent adsorption capability of TiO_2/Co_3O_4-CNTs.

The electrochemical performance of S–TiO_2/Co_3O_4-CNTs was evaluated as demonstrated in figure 5. The initial three CV cycles of the S–TiO_2/Co_3O_4-CNT cathode are depicted in figure 5(a). Two pronounced cathodic peaks at 2.33 V and 2.06 V refer to the transition of sulfur into high-ordered soluble polysulfide (Li_2S_x, $4 \leqslant x \leqslant 8$) and subsequently into low-ordered insoluble Li_2S_2/Li_2S, respectively. Correspondingly, the anodic peak at around 2.38 V represents the reverse reaction of conversion to S_8 in the charging stage [30]. The obtained CV curves are well overlapped upon further cycling, confirming the high reversibility of the S–TiO_2/Co_3O_4-CNTs cathode. The cathodes with and without CNTs in their composition were compared upon cycling at 0.2 C between 1.7 and 2.8 V over 100 cycles (figure 5(b)). As it was expected, the results show improved cycling stability for the S–TiO_2/Co_3O_4-CNTs cathode with a high capacity retention of 950 mAh g^{-1} after 100 cycles, which corresponded to a capacity retention of 82.1%. Although both electrodes exhibited high coulombic efficiency, the S–TiO_2/Co_3O_4 cathode displayed a remarkably lower capacity of 700 mAh g^{-1} along with less stable cycling. The galvanostatic charge/discharge potential profiles of the S–TiO_2/Co_3O_4-CNTs electrode exhibit a two-plateau discharge curve and one charging slope due to the multistep sulfur electrochemistry (figure S3). The potential profile could be well maintained even after 100 cycles, confirming highly reversible electrochemistry of the obtained cathode.

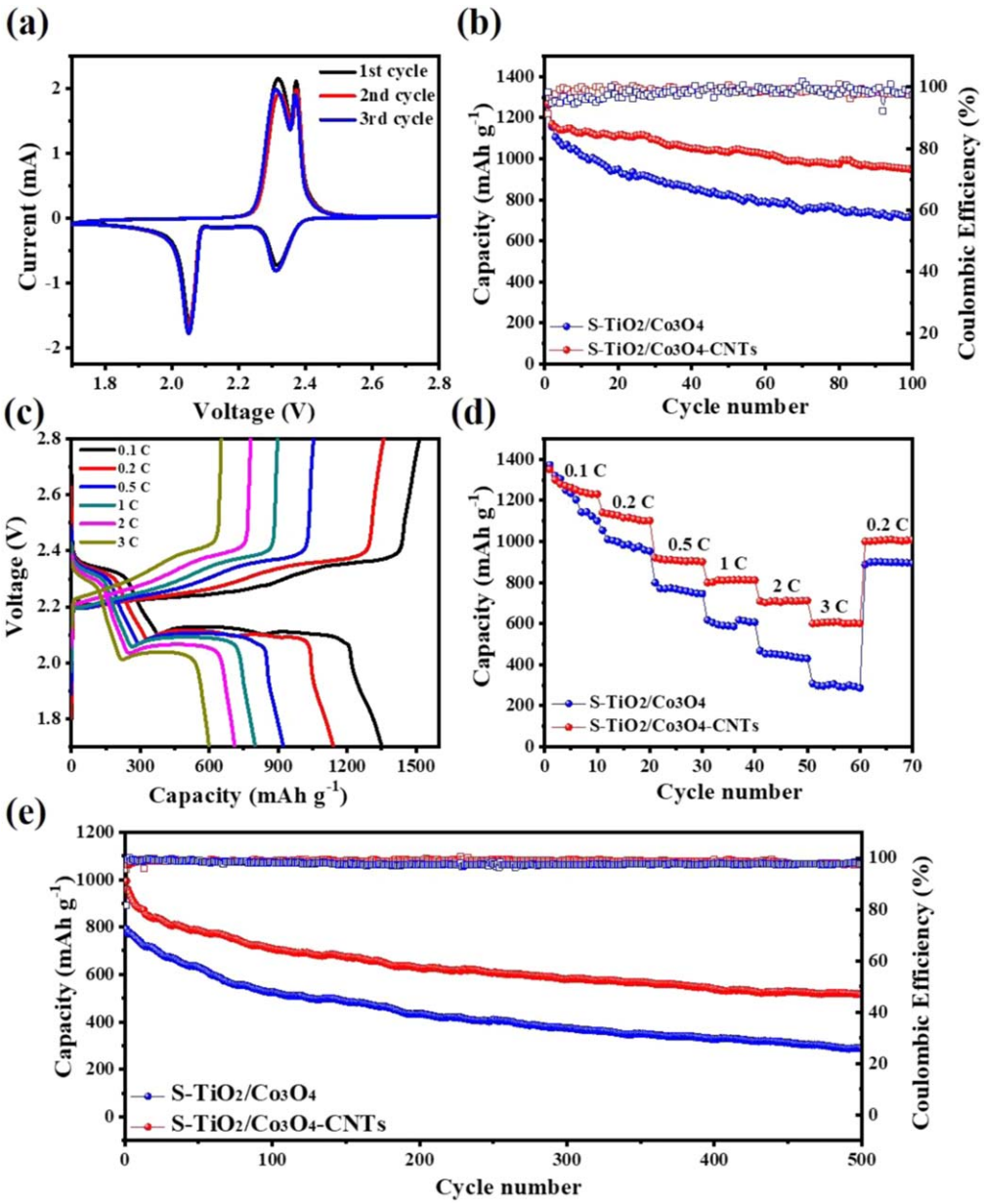

Figure 5. (a) CV curves of S–TiO_2/Co_3O_4-CNTs cathode, (b) cycling performance of S–TiO_2/Co_3O_4 and S–TiO_2/Co_3O_4-CNTs at 0.2 C; (c) discharge/charge profiles of S–TiO_2/Co_3O_4-CNTs cathode at 0.1, 0.2, 0.5, 1.0, 2.0, and 3.0 C; (d) rate capability of S–TiO_2/Co_3O_4-CNTs and S–TiO_2/Co_3O_4 cathodes at 0.1, 0.2, 0.5, 1.0, 2.0, and 3.0 C; (e) specific capacities and coulombic efficiency of S–TiO_2/Co_3O_4-CNTs and S–TiO_2/Co_3O_4 electrodes at 0.5 C.

The galvanostatic charge and discharge potential profiles of the cells with S–TiO_2/Co_3O_4-CNTs cathode upon increasing cycling rates are presented in figure 5(c). Similarly to the CV curves, we can observe a typical two-plateau discharge behavior inherent to the Li–S battery. The distinct discharge/charge curves were maintained even at higher current rates, further implying the superior role of TiO_2/Co_3O_4-CNTs in facilitating the redox reaction of sulfur. Figure 5(d) compares the rate capability of the cells with the S–TiO_2/Co_3O_4 and S–TiO_2/Co_3O_4-CNTs cathodes upon increasing cycling rates from 0.1 to 3 C. The rate performance of the S–TiO_2/Co_3O_4-CNTs cathode is superior and it delivers a high initial capacity of 1350 mAh g^{-1} at 0.1 C, which follows by the reversible capacities of 1148, 923, 803, 712 and 603 mAh g^{-1} at 0.2, 1.0, 2 and 3 C, respectively. After reducing the cycling rate back to 0.2 C, the cell could recover a specific capacity value of 1005 mAh g^{-1}, which corresponds to an 87.5% recovery. By contrast, the cells with S–TiO_2/Co_3O_4 cathode exhibited remarkably lower capacities at all cycling rates.

The long-term cycling performance of the cells with S–TiO_2/Co_3O_4 and S–TiO_2/Co_3O_4-CNTs cathodes were evaluated at 0.5 C (figure 5(e)). The S–TiO_2/Co_3O_4-CNTs could retain a high discharge capacity (511 mAh g^{-1}) even after 500 cycles with a corresponding capacity fading rate of 0.097% per cycle. In contrast, the cells with S–TiO_2/Co_3O_4 delivered only 289 mAh g^{-1} after 500 cycles. The results indicate a remarkably improved Li–S battery performance

with the implementation of the TiO_2/Co_3O_4-CNTs host structure.

4. Conclusions

In summary, in this work, the S–TiO_2/Co_3O_4-CNTs cathode was successfully fabricated via a low-cost and facile synthesis route to significantly improve the overall performance of Li–S battery. The porous TiO_2 matrix, in combination with CNTs void spaces in the constructed TiO_2/Co_3O_4-CNTs host, can provide enough pore volume to store sulfur and efficiently buffer the electrode volume expansion during charge/discharge processes. In such rational structure, LiPS are effectively contained in the system due to the surface chemical absorption by polar TiO_2 and Co_3O_4. As a result, the cells with S–TiO_2/Co_3O_4-CNTs cathode exhibit a high initial capacity of 1270 mAh g^{-1} and a reversible capacity of 950 mAh g^{-1} maintained after 100 cycles at 0.2 C. The designed S–TiO_2/Co_3O_4-CNTs composite could be considered as a promising high-performance cathode material for Li–S battery.

Acknowledgments

This work was supported by Natural Science Foundation of Hebei Province of China (Grant No. B2020202052); Program for the Outstanding Young Talents of Hebei Province, China; Chunhui Project of Ministry of Education of the People's Republic of China (Grant No. Z2017010); the research grants 091019CRP2114 'Three-Dimensional All Solid State Rechargeable Batteries' from Nazarbayev University.

ORCID iDs

Yongguang Zhang https://orcid.org/0000-0001-6584-9062
Gulnur Kalimuldina https://orcid.org/0000-0001-9185-3217
Zhumabay Bakenov https://orcid.org/0000-0003-2781-4955

References

[1] Kremer L S, Hoffmann A, Danner T, Hein S, Prifling B, Westhoff D, Dreer C, Latz A, Schmidt V and Wohlfahrt-Mehrens M 2019 Manufacturing process for improved ultra-thick cathodes in high-energy lithium-ion batteries *Energy Technol.* **8** 1900167
[2] Xiong R, Yang R, Chen Z, Shen W and Sun F 2020 Online fault diagnosis of external short circuit for lithium-ion battery pack *IEEE Trans. Ind. Electron.* **67** 1081–91
[3] Jiang J, Zhu J, Ai W, Wang X, Wang Y, Zou C, Huang W and Yu T 2015 Encapsulation of sulfur with thin-layered nickel-based hydroxides for long-cyclic lithium–sulfur cells *Nat. Commun.* **6** 8622
[4] Peng H J, Zhang Z W, Huang J Q, Zhang G, Xie J, Xu W T, Shi J L, Chen X, Cheng X B and Zhang Q 2016 A cooperative interface for highly efficient lithium–sulfur batteries *Adv. Mater.* **28** 9551–8
[5] Baumann A E, Burns D A, Diaz J C and Thoi V S 2019 Lithiated defect sites in Zr metal-organic framework for enhanced sulfur utilization in Li–S batteries *ACS Appl. Mater. Interfaces* **11** 2159–67
[6] Chen G, Song X, Wang S, Wang Y, Gao T, Ding L-X and Wang H 2018 A multifunctional separator modified with cobalt and nitrogen co-doped porous carbon nanofibers for Li–S batteries *J. Membr. Sci.* **548** 247–53
[7] Zhou L, Li H, Wu X, Zhang Y, Danilov D L, Eichel R-A and Notten P H L 2019 Double-shelled Co_3O_4/C nanocages enabling polysulfides adsorption for high-performance lithium–sulfur batteries *ACS Appl. Energy Mater.* **2** 8153–62
[8] Zhao Z, Wang S, Liang R, Li Z, Shi Z and Chen G 2014 Graphene-wrapped chromium-MOF(MIL-101)/sulfur composite for performance improvement of high-rate rechargeable Li–S batteries *J. Mater. Chem.* A **2** 13509–12
[9] Zhang J, Li Z, Chen Y, Gao S and Lou X W D 2018 Nickel-iron layered double hydroxide hollow polyhedrons as a superior sulfur host for lithium–sulfur batteries *Angew. Chem., Int. Ed. Engl.* **57** 10944–8
[10] Fang R, Chen K, Yin L, Sun Z, Li F and Cheng H M 2019 The regulating role of carbon nanotubes and graphene in lithium-ion and lithium–sulfur batteries *Adv. Mater.* **31** e1800863
[11] Li F, Tao J, Zou Z, Li C, Hou Z and Zhao J 2020 Aminomethyl-functionalized carbon nanotubes as a host of small sulfur clusters for high-performance lithium–sulfur batteries *ChemSusChem* **13** 2761–8
[12] Yan Y, Shi M, Zou Y, Wei Y, Chen L, Fan C, Yang R and Xu Y 2019 Tunable hierarchical porous carbon aerogel/graphene composites cathode matrix for Li–S batteries *J. Alloys Compd.* **791** 952–61
[13] Ji S, Imtiaz S, Sun D, Xin Y, Li Q, Huang T, Zhang Z and Huang Y 2017 Coralline-like N-doped hierarchically porous carbon derived from enteromorpha as a host matrix for lithium–sulfur battery *Chemistry* **23** 18208–15
[14] Hussain S *et al* 2020 Novel gravel-like NiMoO4 nanoparticles on carbon cloth for outstanding supercapacitor applications *Ceram. Int.* **46** 6406–12
[15] Hussain S, Yang X, Aslam M K, Shaheen A, Javed M S, Aslam N, Aslam B, Liu G and Qiao G 2020 Robust TiN nanoparticles polysulfide anchor for Li–S storage and diffusion pathways using first principle calculations *Chem. Eng. J.* **391** 123595
[16] Yao J, Mei T, Cui Z, Yu Z, Xu K and Wang X 2017 Hollow carbon spheres with TiO_2 encapsulated sulfur and polysulfides for long-cycle lithium–sulfur batteries *Chem. Eng. J.* **330** 644–50
[17] Cheng M, Han T, Zhang M, Zhang H, Sun B, Zhu S, Zhai M, Wu Y and Liu J 2020 Hydrogel and sulfur co-coating on semispherical TiO_2 as polysulfides-immobilized cathodes for high capacity and stable rate performance lithium–sulfur batteries *Appl. Surf. Sci.* **513** 145887
[18] Chen Y 2018 Core–shell MnO_2/S composite as high-performance cathode materials for Li–S batteries *Int. J. Electrochem. Sci.* **13** 12155–62
[19] Yang Y, Ma G, Huang J, Nan J, Zhen S, Wang Y and Li A 2020 Hollow MnO_2 spheres/porous reduced graphene oxide as a cathode host for high-performance lithium–sulfur batteries *J. Solid State Chem.* **286** 121297
[20] Jinguo Z 2019 High capacity and long cycle stability lithium–sulfur battery by using hollow Co_3O_4 nanofibers as host materials *Mater. Res. Express* **6** 125512
[21] Zhou Z, Li Y, Fang T, Zhao Y, Wang Q, Zhang J and Zhou Z 2019 MOF-derived Co_3O_4 polyhedrons as efficient

polysulfides barrier on polyimide separators for high temperature lithium–sulfur batteries *Nanomaterials* **9** 1574

[22] Hussain S, Ullah N, Zhang Y, Shaheen A, Javed M S, Lin L, Zulfiqar, Shah S B, Liu G and Qiao G 2019 One-step synthesis of unique catalyst Ni9S8@C for excellent MOR performances *Int. J. Hydrog. Energy* **44** 24525–33

[23] Lu Y Q *et al* 2018 Novel sulfur host composed of cobalt and porous graphitic carbon derived from MOFs for the high-performance Li–S battery *ACS Appl. Mater. Interfaces* **10** 13499–508

[24] Wang R *et al* 2020 Highly dispersed cobalt clusters in nitrogen-doped porous carbon enable multiple effects for high-performance Li–S battery *Adv. Energy Mater.* **10** 1903550

[25] Zhang J, Wang W, Zhang Y, Bakenov Z and Zhao Y 2019 Hierarchical rambutan-like CNTs-assembled N−Co −C@rGO composite as sulfur immobilizer for high-performance lithium–sulfur batteries *ChemElectroChem* **6** 4565–70

[26] Wang H, Yuan X, Wu Y, Zeng G, Chen X, Leng L, Wu Z, Jiang L and Li H 2015 Facile synthesis of amino-functionalized titanium metal-organic frameworks and their superior visible-light photocatalytic activity for Cr(VI) reduction *J. Hazard. Mater.* **286** 187–94.

[27] Liu X, Shao X, Li F and Zhao M 2018 Anchoring effects of S-terminated Ti_2C MXene for lithium–sulfur batteries: a first-principles study *Appl. Surf. Sci.* **455** 522–6

[28] Zhou D, Yang L, Yu L, Kong J, Yao X, Liu W, Xu Z and Lu X 2015 Fe/N/C hollow nanospheres by Fe(iii)-dopamine complexation-assisted one-pot doping as nonprecious-metal electrocatalysts for oxygen reduction *Nanoscale* **7** 1501–9

[29] Liu Y T, Han D D, Wang L, Li G R, Liu S and Gao X P 2019 $NiCo_2O_4$ nanofibers as carbon-free sulfur immobilizer to fabricate sulfur-based composite with high volumetric capacity for lithium–sulfur battery *Adv. Energy Mater.* **9** 1803477

[30] Xiao Z, Li Z, Li P, Meng X and Wang R 2019 Ultrafine Ti_3C_2 MXene nanodots-interspersed nanosheet for high-energy-density lithium–sulfur batteries *ACS Nano* **13** 3608–17